Geophysical Research Letters

RESEARCH LETTER
10.1029/2023GL107232

Phase-Accurate Internal Tides in a Global Ocean Forecast Model: Potential Applications for Nadir and Wide-Swath Altimetry

Badarvada Yadidya[1], Brian K. Arbic[1], Jay F. Shriver[2], Arin D. Nelson[1,3,4], Edward D. Zaron[5], Maarten C. Buijsman[6], and Ritabrata Thakur[1,7]

[1]Department of Earth & Environmental Sciences, University of Michigan, Ann Arbor, MI, USA, [2]Naval Research Laboratory, Stennis Space Center, Stennis Space Center, MS, USA, [3]Graduate School of Oceanography, University of Rhode Island, Kingston, RI, USA, [4]Naval Undersea Warfare Center, Newport, RI, USA, [5]College of Earth, Ocean, and Atmospheric Sciences, Oregon State University, Corvallis, OR, USA, [6]Division of Marine Science, University of Southern Mississippi, Stennis Space Center, MS, USA, [7]Department of Applied Mechanics, Indian Institute of Technology Delhi, New Delhi, India

Abstract Internal tides (ITs) play a critical role in ocean mixing, and have strong signatures in ocean observations. Here, global IT sea surface height (SSH) in nadir altimetry is compared with an ocean forecast model that assimilates de-tided SSH from nadir altimetry. The forecast model removes IT SSH variance from nadir altimetry at skill levels comparable to those achieved with empirical analysis of nadir altimetry. Accurate removal of IT SSH is needed to fully reveal lower-frequency mesoscale eddies and currents in altimeter data. Analysis windows of order 30–120 days, made possible by the frequent (hourly) outputs of the forecast model, remove more IT SSH variance than longer windows. Forecast models offer a promising new approach for global internal tide mapping and altimetry correction. Because they provide information on the full water column, forecast models can also help to improve understanding of the underlying dynamics of ITs.

Plain Language Summary Tidal flow over topographic features on the seafloor generates vertical displacements along the interfaces of ocean layers that have different densities. These vertical displacements at tidal frequencies are known as internal tides. Internal tide displacements are largest well below the sea surface, but also display a sea surface height (SSH) signature that is large enough to be measured by satellite altimeters. Removing internal tide signals from satellite altimeter SSH allows for a more accurate accounting of non-tidal features, including slowly evolving ocean currents and eddies, that are also measured by altimeters. Here, we show that supercomputer ocean forecast simulations of the global internal tide field are able to remove internal tide SSH from satellite altimeter measurements with a skill level that is comparable to the skill of internal tide SSH removal based upon analysis of the satellite altimeter data itself. Thus, forecast models offer a complementary method for this important task. In addition, forecast models provide information on the entire ocean water column, not just the sea surface. Finally, the hourly outputs of forecast models allow for a greater variety of tidal analysis record lengths than can be achieved with altimeter outputs, which report sea surface height fields much less frequently.

Key Points:

- Global ocean forecast models can accurately simulate both long-term (phase-locked) internal tides and their short-term modulations
- Ocean forecast models offer a useful complement to empirical models for mapping internal tides and correcting altimetry for internal tides
- In regions of strong internal tides, optimal variance reduction in nadir altimetry is attained through short-term tidal analyses (~60 days)

Supporting Information:

Supporting Information may be found in the online version of this article.

Correspondence to:

B. Yadidya,
yadidyabadarvada@gmail.com

Citation:

Yadidya, B., Arbic, B. K., Shriver, J. F., Nelson, A. D., Zaron, E. D., Buijsman, M. C., & Thakur, R. (2024). Phase-accurate internal tides in a global ocean forecast model: Potential applications for nadir and wide-swath altimetry. *Geophysical Research Letters*, *51*, e2023GL107232. https://doi.org/10.1029/2023GL107232

Received 10 NOV 2023
Accepted 31 JAN 2024

Author Contributions:

Conceptualization: Badarvada Yadidya, Brian K. Arbic, Jay F. Shriver, Arin D. Nelson, Edward D. Zaron, Maarten C. Buijsman, Ritabrata Thakur
Data curation: Badarvada Yadidya, Jay F. Shriver, Arin D. Nelson
Formal analysis: Badarvada Yadidya, Arin D. Nelson
Funding acquisition: Brian K. Arbic, Maarten C. Buijsman
Investigation: Badarvada Yadidya, Jay F. Shriver, Arin D. Nelson
Methodology: Badarvada Yadidya, Brian K. Arbic, Jay F. Shriver, Arin D. Nelson, Edward D. Zaron, Maarten C. Buijsman, Ritabrata Thakur

© 2024. The Authors.
This is an open access article under the terms of the Creative Commons Attribution License, which permits use, distribution and reproduction in any medium, provided the original work is properly cited.

1. Introduction

This paper is about mapping internal tides with a global ocean forecast model based upon a hydrodynamical core that assimilates ocean observations, and potential applications of the forecasted internal tide fields for satellite altimetry. Internal tides, also known as baroclinic tides, are internal gravity waves of tidal frequency. Internal tides are generated by tidal flow over topographic features such as seamounts, mid-ocean ridges, and continental slopes, which create vertical motions at tidal frequencies along the interfaces of ocean layers that have different densities (Baines, 1982; Bell, 1975; Wunsch, 1975). The vertical displacement signals of internal tides are at their largest well below the sea surface, but the sea surface height (SSH) signal of internal tides is large enough to be measured by satellite altimeters (Carrère et al., 2021; Ray & Mitchum, 1996, 1997). The spatial scales of first vertical mode internal tides in the open ocean are of order 100 km, similar to those of mesoscale eddies. Higher vertical modes have shorter horizontal scales but also have a smaller imprint on SSH. (Vertical normal modes, with differing vertical structure and horizontal scales, are defined from application of a Sturm-Liouville problem to a profile of oceanic stratification; see, e.g., Gill (1982).)

Project administration: Brian K. Arbic
Resources: Brian K. Arbic, Jay F. Shriver
Software: Badarvada Yadidya, Jay F. Shriver, Arin D. Nelson
Supervision: Brian K. Arbic, Jay F. Shriver
Validation: Badarvada Yadidya, Arin D. Nelson
Visualization: Badarvada Yadidya
Writing – original draft: Badarvada Yadidya, Brian K. Arbic
Writing – review & editing: Badarvada Yadidya, Brian K. Arbic, Jay F. Shriver, Edward D. Zaron, Maarten C. Buijsman, Ritabrata Thakur

Internal tides are important for a variety of reasons, including their prominence in *in situ* observational records of the ocean (Arbic, 2022; Luecke et al., 2020; Yu et al., 2019), their impacts on operational oceanography and ocean acoustics, their contributions to the broadband internal gravity wave continuum (Garrett & Munk, 1975) and to internal wave-wave interactions (Dematteis & Lvov, 2021; McComas & Bretherton, 1977; Müller et al., 1986; Olbers, 1976; Pan et al., 2020; Skitka et al., 2023; Solano et al., 2023), and their central importance in mixing the open ocean beneath the mixed layer (Gregg, 1989; Kunze, 2017b; Polzin et al., 1995; Whalen et al., 2015). This subsurface ocean mixing is thought to exert a strong control on oceanic stratification, the meridional overturning circulation, and the storage and transport of heat and carbon in the ocean (Kunze, 2017a; Munk & Wunsch, 1998).

Satellite altimetry has revolutionized many topics within physical oceanography (Abdalla et al., 2021; Fu & Cazenave, 2000; Stammer & Cazenave, 2017) including the study of internal tides (Carrère et al., 2021; Ray & Mitchum, 1996, 1997). The nadir altimeters used by the altimetry community for the past 30 years measure SSH along one-dimensional tracks that are spaced far apart (e.g., ∼300 km for the TOPEX/Jason series). In contrast, the Surface Water and Ocean Topography (SWOT) satellite, which was launched in December 2022, is measuring SSH at much higher horizontal resolutions than nadir altimetry, and in two dimensions rather than just one (Morrow et al., 2019). Nadir altimetry must be accurately corrected for the large-scale surface tides, also known as barotropic tides (Egbert et al., 1994; Ray, 1999), that account for most of the SSH signal measured by altimetry. Accurate removal of the barotropic tides, which have spatial scales of order 1,000 km in the open ocean, allows for mapping of low-frequency SSH signals due to mesoscale eddies, western boundary currents, El Niño, and the rise of mean sea level (Abdalla et al., 2021; Fu & Cazenave, 2000; Stammer & Cazenave, 2017). Because SWOT will measure SSH at smaller spatial scales (Morrow et al., 2019), internal tide corrections will become even more important in the SWOT era. At present, the High Resolution Empirical Tide model (HRET8.1), an empirical model based on analysis of the constellation of nadir altimeters (Zaron, 2019), is being used for internal tide corrections in both nadir altimetry and SWOT. In HRET8.1, the first two vertical modes are captured at M_2, K_1, and O_1 frequencies, whereas only mode one is retained at S_2. Accurate internal tide corrections will be necessary for observing mesoscale and potentially even sub-mesoscale motions within the rich SWOT dataset. In fact, wavenumber spectra of SSH computed from models with simultaneous atmospheric and tidal forcing demonstrate that at the high wavenumbers of interest for SWOT, high-frequency motions such as internal tides and gravity waves can dominate over eddies in some regions (Qiu et al., 2018; Richman et al., 2012; Rocha et al., 2016; Savage et al., 2017; Torres et al., 2018).

We investigate the degree to which an operational tide-resolving ocean forecast system based on the HYbrid Coordinate Ocean Model (HYCOM; Bleck (2002)) can be used to provide accurate predictions of baroclinic tidal SSH. The tide prediction problem is conceptually decomposed into two parts, namely, the prediction of the phase-locked (long-term) internal tide and the prediction of the non-phase-locked, or modulated internal tide, which represents instantaneous departures from the phase-locked internal tide. This decomposition of the prediction problem is natural and provides for a one-to-one comparison with the existing HRET8.1 predictions for the phase-locked part. Furthermore, it exposes the unique advantages of the hydrodynamics-based HYCOM simulation for predicting the modulated tide because HYCOM explicitly resolves the seasonal, mesoscale, and other variability responsible for internal tide modulations. Indeed, we have shown in past work (Nelson et al., 2019) that non-assimilative HYCOM simulations can reproduce geographical patterns of internal tide modulations inferred from the wavenumber spectra of satellite altimetry (Zaron, 2017). Because the HYCOM output examined here is hourly, much more frequent than the 9–35 day revisit times of nadir altimeters (Zaron, 2019), it is possible to use much shorter record lengths (for instance, of order 30–120 days) in analysis of HYCOM output than in analysis of altimeter data. There are rapid spatial modulations, over time scales of order 30 days, in the analysis of internal tides in altimeter data (Zaron, 2022). This fluctuation period is comparable to the order 10–30 day decorrelation times of mesoscale eddies (Stammer, 1997).

The operational tide simulation builds upon recent simulations of HYCOM that have employed astronomical tidal forcing alongside atmospheric forcing (e.g., Arbic, 2022; Arbic et al., 2010, 2012, 2018; Buijsman et al., 2020; Shriver et al., 2012, among many others). Thus far, the HYCOM tides papers have focused on forward (non-assimilative) HYCOM solutions [an Augmented State Ensemble Kalman Filter (ASEnKF) (Ngodock et al., 2016) is employed to improve the barotropic tides in HYCOM, but the ASEnKF does not involve direct assimilation of altimeter SSH fields into HYCOM]. The geographical patterns of the internal tide SSH (Ansong et al., 2015; Buijsman et al., 2020; Shriver et al., 2012) and near-surface tidal kinetic energy (Arbic et al., 2022) in non-assmilative HYCOM closely resemble those in altimetry and surface drifters, respectively, as seen in visual

comparisons and basin- or global averages of amplitudes. The question arises as to whether the internal tides in HYCOM are "phase-accurate"–in other words, whether the phases and amplitudes of individual peaks and troughs in the HYCOM internal tide fields match those in altimetry. Carrère et al. (2021) showed that the skill of non-data assimilative HYCOM solutions in removing internal tide SSH variance in altimeter records is noticeably less than the skill of empirical internal tide models. However, the phase accuracy of internal tides in data-assimilative HYCOM forecasts has not yet been quantified in the literature - that is indeed what we will do here.

2. Data and Methods

2.1. Jason-2 Altimetry

We used 3 years (2017–2019) of along-track Jason-2 altimeter measurements extracted from the Radar Altimetry Database System (RADS; http://rads.tudelft.nl/rads/rads.shtml). All standard corrections, such as those for environmental path delays, the inverse barometer effect, sea-state bias, mean sea level, solid Earth tides, and barotropic tides, have been applied. No internal tide correction is applied because our goal is to compare HRET8.1 with HYCOM for this purpose.

2.2. HYCOM

The US Navy has been actively running global data-assimilative HYCOM simulations for operational purposes over the past two decades (Chassignet et al., 2009). The main objective of the data-assimilation systems (Cummings & Smedstad, 2013) is the accurate representation of mesoscale eddies (Chassignet et al., 2009) but it also improves the background stratification (Luecke et al., 2020), a critical factor in internal tide modeling. Here we use a data-assimilative global HYCOM simulation (EXPT 21.6) that was run on a tri-polar grid at 1/25° horizontal resolution (∼3 km in mid-latitudes) with 41 hybrid vertical layers. The hybrid vertical coordinate (Bleck, 2002) smoothly transitions between z (depth) coordinates in the open-ocean upper mixed layer, density (isopycnal) coordinates in the open-ocean beneath the upper mixed layer, and terrain-following coordinates in coastal regions. Data assimilation in this HYCOM run relies on the NCODA system (Cummings & Smedstad, 2013), which employs a 24-hr assimilation window and a 3-hr Incremental Analysis Update interval. The NCODA system adopts a 3D variational (3DVAR) approach, utilizing the daily mean of a short-term HYCOM forecast as a preliminary estimate (background field). It also assimilates a range of observational data, including de-tided satellite altimeter measurements, satellite-based and *in situ* sea surface temperature data, and temperature and salinity profiles collected from eXpendable BathyThermographs, Argo floats, and moored buoys. By design, the tidal signals are effectively filtered out during data assimilation through the use of the daily mean forecast which is intended to provide accurate initialization of the low-frequency ocean state (seasonal and mesoscale variability). Astronomical tidal forcing, consisting of the M_2, S_2, N_2, K_1, and O_1 tidal constituents, is integrated into the simulations. A topographic wave drag scheme (Jayne & St. Laurent, 2001), accounting for the breaking of fine-scale internal waves that are unresolved in the situations and that are generated by flows over topography, is tuned to minimize barotropic tidal errors with respect to TPXO (Egbert et al., 1994). Application of the ASEnKF decreases the global root mean square error of the M_2 barotropic tide with respect to TPXO, in waters deeper than 1,000 m and equatorward of 66°, to about 2.6 cm (Ngodock et al., 2016). The atmospheric forcing is derived from the Navy Global Environmental Model (NAVGEM; Hogan et al. (2014)), which includes 60 layers extending up to 19 km in altitude and employs a horizontal resolution of 0.17°. HYCOM utilizes relative winds over the ocean surface to compute surface wind stress, and the atmospheric forcing is applied every 3 hrs. The K-profile parameterization (KPP) scheme is used as the subgrid-scale vertical mixing model. Our analysis in this paper is based on hourly model data from January 2017 to December 2019, covering a span of 3 years.

In order to examine the predictability of internal tides, it is necessary to separate the large-scale barotropic tides from the small-scale internal tides in HYCOM output. Until recently, we have used steric and non-steric SSH, which HYCOM routinely outputs, to respectively represent smaller-scale and larger-scale motions (Savage et al., 2017). However, Zaron and Ray (2023) demonstrated that the steric/non-steric SSH split is not optimal. We therefore separate the two classes of motions with a spatial filter, akin to the along-track high-pass filtering used in (Ray & Mitchum, 1996, 1997) but acting in two dimensions instead of one. We define the "Filtered SSH" as the low-passed output of a 2-dimensional Gaussian filter applied to the total SSH from HYCOM. In this paper, semidiurnal internal tides are extracted using a characteristic wavelength of 300 km, while for diurnal internal tides, the chosen characteristic wavelength is 600 km. To prevent any artifacts resulting from the application of

the spatial filter, gridpoints shallower than 1,500 m are excluded from the analysis. Consistent with the arguments of Zaron and Ray (2023), we find that the prediction skill of Filtered SSH exceeds that of steric SSH (Figure S1 in Supporting Information S1).

2.3. Harmonic Analysis and Variance Reduction Statistics

After interpolating the HYCOM Filtered SSH onto nadir altimeter track points, we extract the internal tide signal at semidiurnal (M_2, S_2, N_2) and diurnal (K_1, O_1) frequencies via tidal harmonic analysis using multiple time windows, including 15, 30, 60, 90, 120, 150, 180, 210 days, and 3 years. We will denote the 15, 30, 60, 90, 120, 150, 180, and 210 days analysis windows as "shorter time windows." The 3 year analysis of HYCOM represents its best estimate of the long-term phase-locked internal tide signal (Ansong et al., 2015; Buijsman et al., 2020), most directly comparable to HRET8.1.

A sliding harmonic analysis is used for shorter time windows. For example, for a 60 days time window, to reconstruct SSH at May 31, 00:00, the harmonic analysis window was considered from May 1, 00:00 to June 30, 00:00 (30 days on either side). At the temporal endpoints, the time window was either started from the first point (i.e., 1 January 2017) or ended with 31 December 2019. After extracting the amplitude and phase, the time-series is reconstructed at every time-step of altimeter observations.

We define variance reduction as a measure of how much either model, HRET8.1 or HYCOM, reduces the variance of the SSH in the nadir altimetry. We computed variance reduction following the method of Zaron (2019), who compared HRET with nadir altimetry, and Carrère et al. (2021), who compared non-data assimilative HYCOM and several empirical models with nadir altimetry, using

$$\text{Variance reduction} = \text{Var}(SSH_{Altimetry}) - \text{Var}(SSH_{Altimetry} - SSH_{Model}) \quad (1)$$

where "Var" represents the variance, $SSH_{Altimetry}$ is the time series of total SSH (including internal tidal motions) from nadir altimetry, and SSH_{Model} is the time series of internal tide SSH constructed from the amplitudes and phases extracted from analysis of either HRET8.1 or HYCOM. HRET8.1 is regridded on to nadir altimeter track points before computing variance reduction. Note that HRET8.1 removes variance only at M_2, S_2, K_1, O_1 frequencies, whereas HYCOM can additionally remove N_2 variance.

3. Results

A global map of M_2 internal tide SSH amplitudes in HYCOM is presented in Figure 1a. The map is constructed after regridding the data from altimeter track points to a uniform 0.5° latitude-longitude grid. A visual comparison of individual M_2 internal tide SSH peaks and troughs (Figure 1b) in HRET8.1 and the 3-year HYCOM analysis in the HAWAII region, demonstrates that HYCOM can replicate the spatial variability of internal tide amplitudes and phases with reasonable accuracy.

HYCOM is able to reproduce the geographical pattern of phase-locked internal tide SSH variance reduction seen in HRET8.1 at both semidiurnal and diurnal frequencies (Figures 2a–2d). As will be shown below, the HYCOM variance reduction for the total tide, the sum of the phase-locked and modulated components, exceeds that of HRET8.1 in some regions, especially those with strong internal tides. It appears that there are more regions where variance is added to altimetry in the HYCOM analysis, especially where mesoscale eddies are relatively strong, and especially for shorter tidal analysis time windows (Figure S2 in Supporting Information S1).

The above qualitative description of the phase-locked tide in HYCOM is made precise in the 3-year results of the statistical summary in Figure 3. In the regions considered, HYCOM explains only a little less–by about 10%–30%–of the phase-locked variance explained by HRET8.1 (Figure 3; refer only to the 3-year HYCOM results for this point). This remarkable level of skill reflects the ability of HYCOM to simulate the time-average stratification and barotropic tide, which together with topography determine the phase-locked baroclinic tides.

We now discuss the total (phase-locked plus modulated) internal tide in different regions. The presence of steep submarine ridges and strong barotropic tidal currents in the Luzon Strait establishes it as one of the world's most dynamic locations for barotropic-to-baroclinic energy conversion in the ocean (e.g., Arbic et al., 2012; Buijsman et al., 2010, 2014; Egbert & Ray, 2000; Niwa & Hibiya, 2004). HYCOM's variance reduction in this region

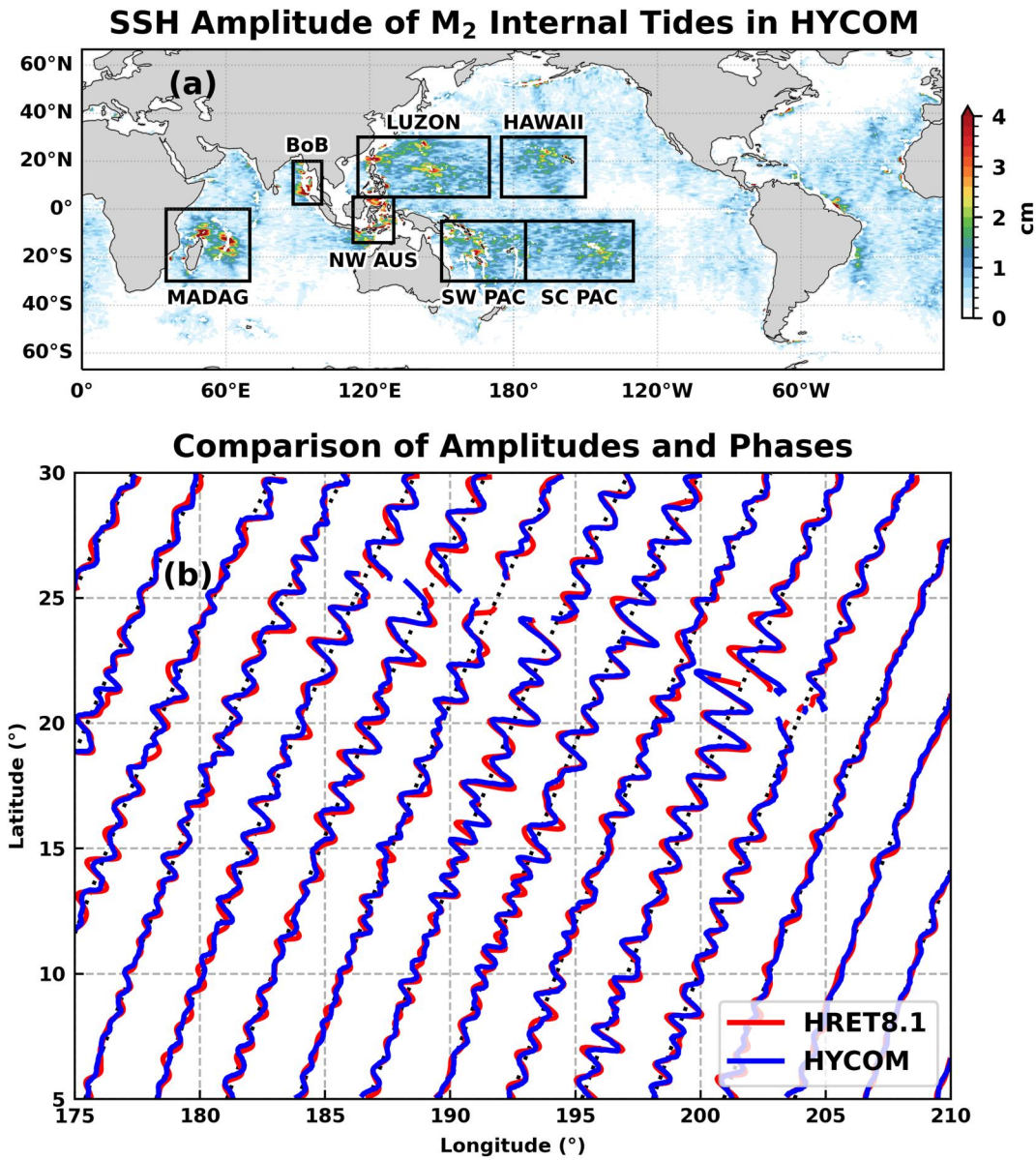


Figure 1. (a) Amplitude of M_2 internal tide SSH fields extracted from 3-year harmonic analysis of HYCOM. Boxes represent regions with strong internal tide activity: region near Luzon Strait (LUZON), region near Hawaii Islands (HAWAII), region near Madagascar Island (MADAG), Southwest Pacific (SW PAC), Southcentral Pacific (SC PAC), Bay of Bengal (BoB), and region above Northwest Australia (NW AUS). Regions shallower than 1,500 m are masked out. (b) Comparison of M_2 phase-locked internal tides in terms of quadrature waveform (imaginary part of harmonic constants)–in other words, (amplitude * sin(phase))–between HRET8.1 and the 3-year analysis of HYCOM, for ascending tracks in the HAWAII region.

(including both phase-locked and modulated internal tides) exceeds HRET8.1 (which only includes phase-locked tides) by 25.5%. The inclusion of N_2 further boosts HYCOM's total variance reduction, which then exceeds HRET8.1 by 35.6% (Figure 3). LUZON is a unique region, which contains not only the most powerful semi-diurnal internal tides and but also the strongest diurnal internal tides (Figures 2c and 2d). The large-scale seasonal variability in the Luzon Strait (Zhao & Qiu, 2023) could be responsible for the increased variance reduction due to modulated internal tides by HYCOM.

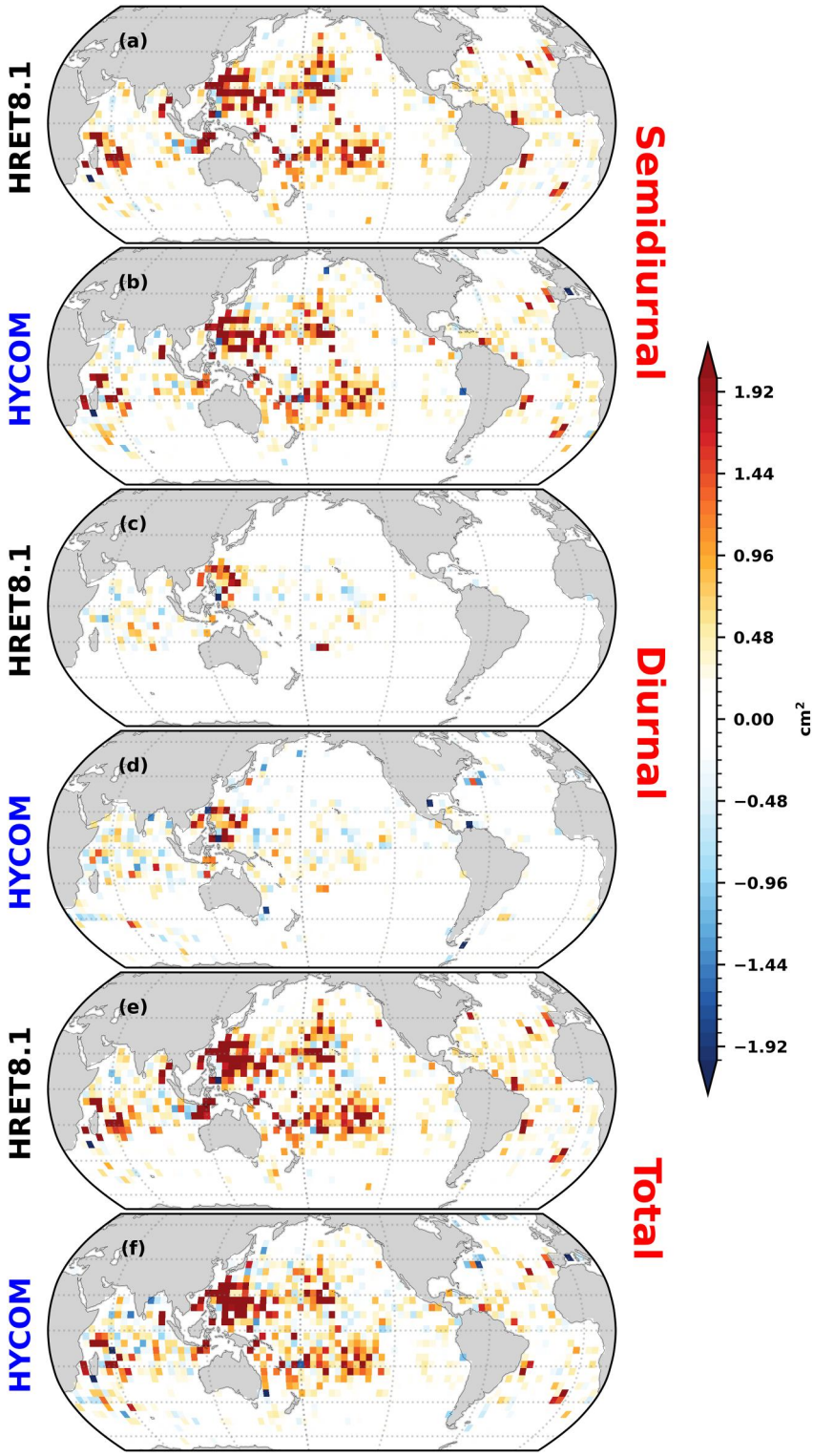


Figure 2. Global maps of internal tide SSH variance reduction in nadir altimetry by HRET8.1 (a, c, e) and HYCOM (b, d, f) at semidiurnal frequency (a, b), diurnal frequency (c, d) and their total [sum of semdiurnal and diurnal] (e, f). The HYCOM results are from the harmonic analysis applied over 3-years. The results are averaged over 4° bins for visualization; fine-scale features can be seen in plots where this bin-averaging is not performed (Figure S2 in Supporting Information S1).

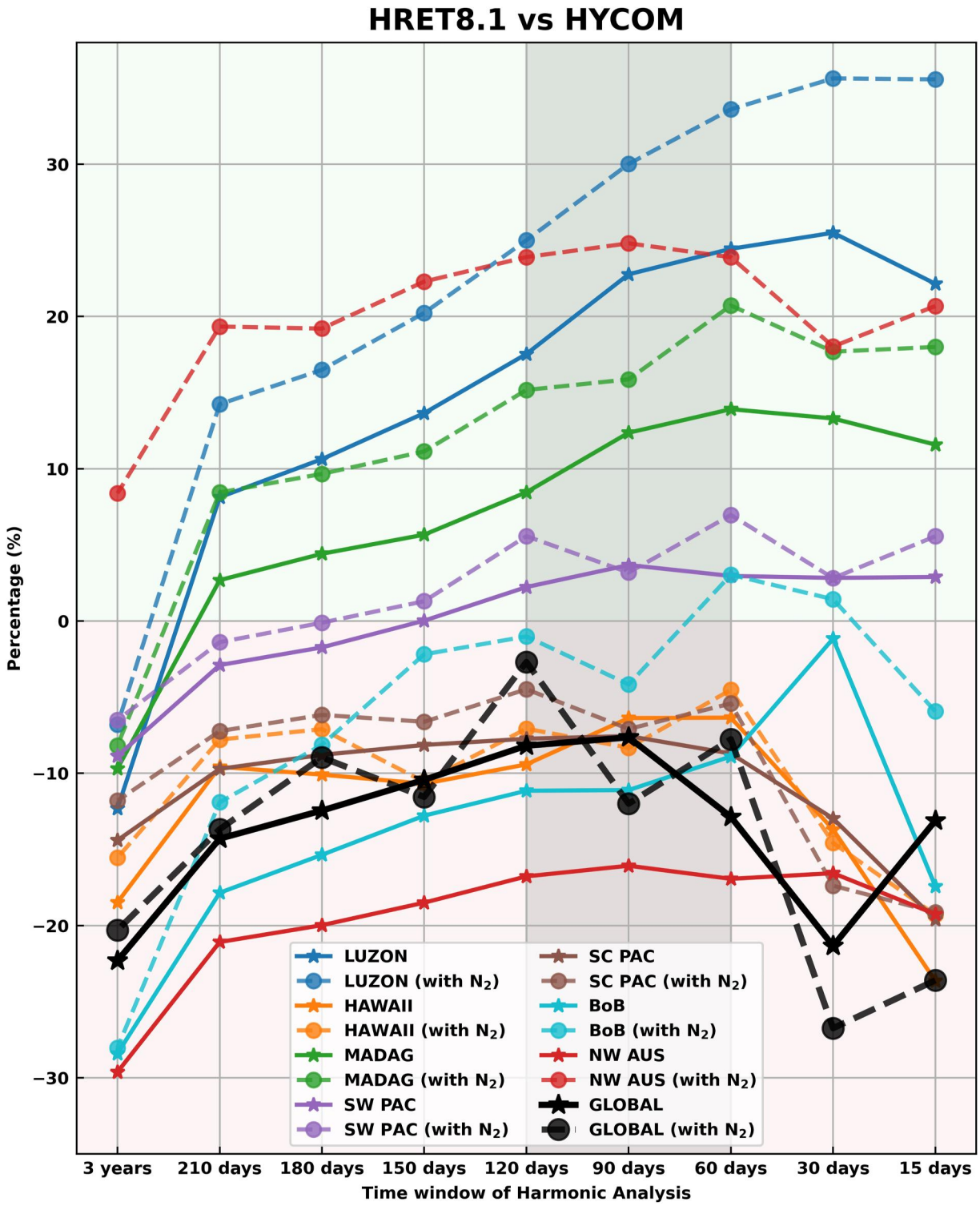


Figure 3. Comparison of variance reduction achieved in HYCOM versus HRET8.1, as a function of the time window of the HYCOM harmonic analysis, measured in percentages. Results are given for the regions of strong internal tide activity shown in Figure 1 as well as for the global average. Positive values imply that HYCOM reduced a larger amount of variance, while negative values imply that HYCOM reduced a smaller amount of variance. The results shown in this figure are computed over both semidiurnal and diurnal bands. Results are shown with and without the inclusion of the N_2 constituent in HYCOM.

Turning to other regions, the majority of energy converted from barotropic tides propagates away from the Hawaiian Ridge in the form of low-mode internal tides instead of dissipating locally (e.g., Carter et al., 2008; Chavanne et al., 2010; Zhao et al., 2010). HRET8.1 reduces slightly more internal tide SSH variance than HYCOM in the HAWAII region (6.3%), even when N_2 (4.5%) is accounted for. The presence of a numerical instability in the high-latitude North Pacific, lying above the Hawaiian region, in HYCOM (e.g., Arbic et al., 2022; Buijsman et al., 2016, 2020) could be part of the reason. Strong barotropic tidal currents flowing perpendicular to the Mascarene ridge can cause internal tides (Da Silva et al., 2015) with associated vertical displacements as large as 160 m (Morozov, 2006). In MADAG, HYCOM removes 13.9% and 20.7% more variance compared to HRET8.1, without and with N_2, respectively. The presence of the Solomon archipelago plays a key role in generating the internal tides in SW PAC (e.g., Niwa & Hibiya, 2001, 2011; Tchilibou et al., 2020). HYCOM reduces 3.7% more variance in SW PAC, and 7% more when N_2 is included. HYCOM's performance in SC PAC, where the shelf-slope regions of the French Polynesian Islands are the main generation sites, lags behind HRET8.1 by 7.5%. Strong stratification and complex bathymetry along the Andaman Nicobar Ridge makes BoB a strong region for internal tides (e.g., Yadidya and Rao, 2022a, 2022b; Yadidya et al., 2022). HYCOM removed 3% more variance in BoB when N_2 is included. The dynamic interplay of Pacific and Indian Ocean tidal forces within the Indonesian Seas (NW AUS) manifests intricate baroclinic tidal fields (e.g., Ray et al., 2005; Robertson & Ffield, 2008). HYCOM removed 16%–29% less variance without N_2 but after its inclusion, HYCOM removed 8%–25% more variance than HRET8.1. In regions with weaker amplitude, far-field internal tides, such as the Northeast Pacific Ocean (15°N–45°N, 135°W–120°W), East Pacific Ocean (35°S–10°N, 100°W–70°W) and Atlantic Ocean (40°S–40°N, 60°W–0°E), HRET8.1 does a relatively better job than HYCOM (Figure S3 in Supporting Information S1), with about 50% greater reduction in variance.

Globally averaged (GLOBAL, Figure 3) results show that HYCOM removes 80% of the phase-locked internal tide when compared to HRET8.1. Shorter time windows (120 days, with N_2) yield 97.5% of the variance that HRET8.1 removes, but HYCOM analyses over 90 days or shorter are less productive, in contrast to the results in regions with strong internal tides. This is likely due to the difficulty of modeling internal tides far from their generation sites (Figure S3 in Supporting Information S1). In contrast, HYCOM performs better in capturing the modulated internal tide signal attributed to intra-seasonal (60–210 days) and mesoscale eddy (15–30 days) modulations near the generation sites.

The principal advantage of using an operational forecast system is that it has the potential to represent the modulated tide not present in HRET8.1. The HYCOM system exhibits considerable skill, although its performance varies regionally (Figure 3). The skill of the HYCOM tidal forecast based on 60–120 days windows exceeds that of the 3-year analysis. In a small number of regions, the 30-day analysis yields even greater variance reduction. Inclusion of the modulated tide in the HYCOM prediction boosts its explained variance by more than 35% in the LUZON region, and about 10%–20% across all regions with strong internal tides (Figure 3). The data assimilation used in the HYCOM forecast system is successful in capturing the time-varying propagation environment responsible for the modulation of the baroclinic tides in the ocean. The inclusion of N_2, which is absent in HRET8.1, generally removed more variance in altimetry for 60-day, 120-day and 3-year analysis (Figure 3). On the other hand, the skill of HYCOM in far-field regions, located a long distance from internal tide generation regions, is notably lower than HRET8.1.

4. Conclusions

We evaluated the potential of data-assimilative HYCOM ocean forecast simulations to map internal tide SSH fields and to serve as an internal tide SSH correction model for satellite altimetry. As measured by its ability to reduce internal tide SSH variance in altimetry, HYCOM reproduces internal tide amplitudes and phases with a skill level comparable to that of the empirical HRET8.1 internal tide model, especially in regions with strong internal tides. Because of the high (hourly) frequency of the HYCOM simulation output, we can use relatively short analysis windows (as little as 15 days) to analyze HYCOM output while still retaining many samples over time. This contrasts with JASON series nadir altimeter data, which is sampled much less frequently (every 9.9 days). A tidal harmonic analysis window of 60 days, comparable to the decorrelation timescales of oceanic mesoscale eddies, consistently achieved the highest variance reduction across all strong internal tide regions. HYCOM achieves somewhat higher internal tide SSH variance reduction than HRET8.1 in LUZON (25.5%), SW PAC (3.7%), and MADAG (13.9%). HYCOM underperforms HRET8.1 by ∼8% in the central Pacific Ocean regions of HAWAII and SC PAC. The inclusion of N_2 in HYCOM moderately increased variance reduction in

most regions (~2%–10%). However, a considerable improvement (~40%) is observed in NW AUS, where the impact of N_2 is most significant (Zhao, 2023).

Our research shows that a data-assimilative forecast system based on HYCOM can provide accurate predictions of the internal tide, capturing both the phase-locked (long-term) and non-phase-locked (modulated) internal tides. The predictions of the phase-locked internal tide with HYCOM are somewhat less accurate than those of an empirical model, HRET8.1, but because HYCOM predictions arise from an ocean forecast model, they can be used to provide insight into internal tide dynamics and their predictability. In contrast, we demonstrated the capacity, in hindcast mode, for making skillful predictions of the modulated tides, something that is not possible with HRET8.1 or any other empirical model of the phase-locked internal tide.

This initial investigation suggests many avenues for follow-up work. One immediate approach to improving baroclinic tide predictions, and crucial for the interpretation of SWOT data, could involve combining the tidal predictions of HYCOM and HRET8.1 by taking the modulated tides from the former and the phase-locked tides from the latter. Based on Figure 3, this strategy should lead to immediate and significant gains of 15%–40% in explained variance in regions with strong internal tide activity. Alternatively, HYCOM could be used as an alternative stand-alone internal tide model, complementary to HRET8.1. The advantages of a HYCOM system would include greater variance reduction in some regions (due to inclusion of modulated internal tides), inclusion of the N_2 tidal constituent (although this will be included in newer versions of HRET), and the ability to examine sub-surface dynamics. Disadvantages of HYCOM internal tide predictions include errors in stratification, bathymetry, and barotropic tidal fields, yielding less accurate phase-locked internal tide (at present) as well as relatively less variance reduction in regions with weaker internal tide signal. The results of this study highlight considerable regional variability in the skill of HYCOM, which requires further investigation. Other salient questions are: what is the upper limit on the modulated tidal variability that can be captured by HYCOM? And: can the results be replicated within the operational forecast system, rather than in hindcast mode, as was done here? In addition, further investigation is required to better understand the underlying dynamics behind the skill of HYCOM predictions. Do shorter analysis windows yield greater variance reduction largely because of seasonal effects, mesoscale effects, or some combination? To what extent is the answer to this question regionally dependent? Why do very short (~15 days) windows generally perform less well than 60-day windows? Is it because such windows are too short to discriminate between internal tides and the powerful, ever-present mesoscale eddy field? Again, more investigation is required to understand these questions which have arisen from this first look at the skill of global-scale internal tide forecast models.

Acronyms

ASEnKF: Augmented State Ensemble Kalman Filter

HRET8.1: High Resolution Empirical Tide (version 8.1)

IT: internal tide

HYCOM: HYbrid Coordinate Ocean Model

NAVGEM: Navy Global Environmental Model

NCODA: Navy Coupled Ocean Data Assimilation system

RADS: Radar Altimetry Database System

SSH: sea surface height

SWOT: Surface Water and Ocean Topography

Data Availability Statement

The post-processed HYCOM data and the Python code to reproduce the analysis shown in this manuscript are provided in Yadidya (2023). The raw HYCOM data can be accessed via OSiRIS (2024) by searching for "GLOBUS OSIRIS Mapped Collection WSU 01."

Acknowledgments
We greatly appreciate two anonymous reviewers for their insightful feedback, significantly enhancing the quality of our manuscript. We thank Richard Ray for valuable discussions and encouragement. BKA thanks Carl Wunsch for valuable input on terminology and emphasis. The satellite altimeter data is sourced from the Radar Altimetry Database System (RADS; http://rads.tudelft.nl/rads/rads.shtml) and processed by EDZ. BY, BKA, JFS, and MCB acknowledge funding support from Office of Naval Research (ONR) Grants N00017-22-1-2576 (BY, BKA, MCB) and N0001423WX01413 (JFS), which are components of the Global Internal Waves project of the National Oceanographic Partnership Program (https://nopp-giw.ucsd.edu/). BKA, ADN, JFS, MCB, and RT also acknowledge funding from NASA Grants NNX17AH55G, and 80NSSC20K1135. RT and BKA acknowledge support from National Science Foundation (NSF) Grant OCE-1851164. EDZ acknowledges support for this work from NASA Grants 80NSSC21K1189 and 80NSSC21K0346. This research was supported in part through computational resources and services provided by Advanced Research Computing at the University of Michigan, Ann Arbor, a grant of computer time from the Department of Defense (DoD) High Performance Computing Modernization Program at the Navy DoD Supercomputing Resource Center, computing resources provided by the NASA Advanced Supercomputing (NAS) Division of the Ames Research Center, and an allotment of storage by the OSiRIS project at University of Michigan. This is NRL contribution NRL/JA/7320-23-6196 and has been approved for public release.

References

Abdalla, S., Abdeh Kolahchi, A., Ablain, M., Adusumilli, S., Aich Bhowmick, S., Alou-Font, E., et al. (2021). Altimetry for the future: Building on 25 years of progress. *Advances in Space Research*, *68*(2), 319–363. https://doi.org/10.1016/j.asr.2021.01.022

Ansong, J. K., Arbic, B. K., Buijsman, M. C., Richman, J. G., Shriver, J. F., & Wallcraft, A. J. (2015). Indirect evidence for substantial damping of low-mode internal tides in the open ocean. *Journal of Geophysical Research: Oceans*, *120*(9), 6057–6071. https://doi.org/10.1002/2015JC010998

Arbic, B. K. (2022). Incorporating tides and internal gravity waves within global ocean general circulation models: A review. *Progress in Oceanography*, *206*, 102824. https://doi.org/10.1016/j.pocean.2022.102824

Arbic, B. K., Alford, M. H., Ansong, J. K., Buijsman, M. C., Ciotti, R. B., Farrar, J. T., et al. (2018). A primer on global internal tide and internal gravity wave continuum modeling in HYCOM and MITgcm. In E. P. Chassignet, A. Pascual, J. Tintoré, & J. Verron (Eds.), *New frontiers in operational oceanography*. GODAE OceanView.

Arbic, B. K., Elipot, S., Brasch, J. M., Menemenlis, D., Ponte, A. L., Shriver, J. F., et al. (2022). Near-surface oceanic kinetic energy distributions from drifter observations and numerical models. *Journal of Geophysical Research: Oceans*, *127*(10), e2022JC018551. https://doi.org/10.1029/2022JC018551

Arbic, B. K., Richman, J., Shriver, J., Timko, P., Metzger, J., & Wallcraft, A. (2012). Global modeling of internal tides within an eddying ocean general circulation model. *Oceanography*, *25*(2), 20–29. https://doi.org/10.5670/oceanog.2012.38

Arbic, B. K., Wallcraft, A. J., & Metzger, E. J. (2010). Concurrent simulation of the eddying general circulation and tides in a global ocean model. *Ocean Modelling*, *32*(3), 175–187. https://doi.org/10.1016/j.ocemod.2010.01.007

Baines, P. G. (1982). On internal tide generation models. Deep Sea Research Part A. *Oceanographic Research Papers*, *29*(3), 307–338. https://doi.org/10.1016/0198-0149(82)90098-X

Bell, T. H. (1975). Topographically generated internal waves in the open ocean. *Journal of Geophysical Research*, *80*(3), 320–327. https://doi.org/10.1029/JC080i003p00320

Bleck, R. (2002). An oceanic general circulation model framed in hybrid isopycnic-Cartesian coordinates. *Ocean Modelling*, *4*(1), 55–88. https://doi.org/10.1016/S1463-5003(01)00012-9

Buijsman, M. C., Ansong, J. K., Arbic, B. K., Richman, J. G., Shriver, J. F., Timko, P. G., et al. (2016). Impact of parameterized internal wave drag on the semidiurnal energy balance in a global ocean circulation model. *Journal of Physical Oceanography*, *46*(5), 1399–1419. https://doi.org/10.1175/JPO-D-15-0074.1

Buijsman, M. C., Kanarska, Y., & McWilliams, J. C. (2010). On the generation and evolution of nonlinear internal waves in the South China Sea. *Journal of Geophysical Research*, *115*(C2), 2009JC005275. https://doi.org/10.1029/2009JC005275

Buijsman, M. C., Klymak, J. M., Legg, S., Alford, M. H., Farmer, D., MacKinnon, J. A., et al. (2014). Three-dimensional double-ridge internal tide resonance in Luzon strait. *Journal of Physical Oceanography*, *44*(3), 850–869. https://doi.org/10.1175/JPO-D-13-024.1

Buijsman, M. C., Stephenson, G. R., Ansong, J. K., Arbic, B. K., Green, J. A. M., Richman, J. G., et al. (2020). On the interplay between horizontal resolution and wave drag and their effect on tidal baroclinic mode waves in realistic global ocean simulations. *Ocean Modelling*, *152*, 101656. https://doi.org/10.1016/j.ocemod.2020.101656

Carrère, L., Arbic, B. K., Dushaw, B., Egbert, G., Erofeeva, S., Lyard, F., et al. (2021). Accuracy assessment of global internal-tide models using satellite altimetry. *Ocean Science*, *17*(1), 147–180. https://doi.org/10.5194/os-17-147-2021

Carter, G. S., Merrifield, M. A., Becker, J. M., Katsumata, K., Gregg, M. C., Luther, D. S., et al. (2008). Energetics of M2 barotropic-to-baroclinic tidal conversion at the Hawaiian Islands. *Journal of Physical Oceanography*, *38*(10), 2205–2223. https://doi.org/10.1175/2008JPO3860.1

Chassignet, E., Hurlburt, H., Metzger, E. J., Smedstad, O., Cummings, J., Halliwell, G., et al. (2009). US GODAE: Global ocean prediction with the HYbrid Coordinate Ocean Model (HYCOM). *Oceanography*, *22*(2), 64–75. https://doi.org/10.5670/oceanog.2009.39

Chavanne, C., Flament, P., Carter, G., Merrifield, M., Luther, D., Zaron, E., & Gurgel, K.-W. (2010). The surface expression of semidiurnal internal tides near a strong source at Hawaii. Part I: Observations and numerical predictions. *Journal of Physical Oceanography*, *40*(6), 1155–1179. https://doi.org/10.1175/2010JPO4222.1

Cummings, J. A., & Smedstad, O. M. (2013). Variational data assimilation for the global ocean. In S. K. Park & L. Xu (Eds.), *Data assimilation for atmospheric, oceanic and hydrologic applications* (Vol. II, pp. 303–343). Springer Berlin Heidelberg. https://doi.org/10.1007/978-3-642-35088-7_13

Da Silva, J., Buijsman, M., & Magalhaes, J. (2015). Internal waves on the upstream side of a large sill of the Mascarene ridge: A comprehensive view of their generation mechanisms and evolution. *Deep Sea Research Part I: Oceanographic Research Papers*, *99*, 87–104. https://doi.org/10.1016/j.dsr.2015.01.002

Dematteis, G., & Lvov, Y. V. (2021). Downscale energy fluxes in scale-invariant oceanic internal wave turbulence. *Journal of Fluid Mechanics*, *915*, A129. https://doi.org/10.1017/jfm.2021.99

Egbert, G. D., Bennett, A. F., & Foreman, M. G. G. (1994). TOPEX/POSEIDON tides estimated using a global inverse model. *Journal of Geophysical Research*, *99*(C12), 24821–24852. https://doi.org/10.1029/94JC01894

Egbert, G. D., & Ray, R. D. (2000). Significant dissipation of tidal energy in the deep ocean inferred from satellite altimeter data. *Nature*, *405*(6788), 775–778. https://doi.org/10.1038/35015531

Fu, L.-L., & Cazenave, A. (2000). *Satellite altimetry and Earth sciences: A handbook of techniques and applications*. Elsevier. (Google-Books-ID: vMu29usEgb0C).

Garrett, C., & Munk, W. (1975). Space-time scales of internal waves: A progress report. *Journal of Geophysical Research*, *80*(3), 291–297. https://doi.org/10.1029/jc080i003p00291

Gill, A. (1982). *Atmosphere-ocean dynamics*. Academic Press.

Gregg, M. C. (1989). Scaling turbulent dissipation in the thermocline. *Journal of Geophysical Research*, *94*(C7), 9686–9698. https://doi.org/10.1029/jc094ic07p09686

Hogan, T., Liu, M., Ridout, J., Peng, M., Whitcomb, T., Ruston, B., et al. (2014). The Navy global environmental model. *Oceanography*, *27*(3), 116–125. https://doi.org/10.5670/oceanog.2014.73

Jayne, S. R., & St. Laurent, L. C. (2001). Parameterizing tidal dissipation over rough topography. *Geophysical Research Letters*, *28*(5), 811–814. https://doi.org/10.1029/2000GL012044

Kunze, E. (2017a). The internal-wave-driven meridional overturning circulation. *Journal of Physical Oceanography*, *47*(11), 2673–2689. https://doi.org/10.1175/JPO-D-16-0142.1

Kunze, E. (2017b). Internal-wave-driven mixing: Global geography and budgets. *Journal of Physical Oceanography*, *47*(6), 1325–1345. https://doi.org/10.1175/JPO-D-16-0141.1

Luecke, C. A., Arbic, B. K., Richman, J. G., Shriver, J. F., Alford, M. H., Ansong, J. K., et al. (2020). Statistical comparisons of temperature variance and kinetic energy in global ocean models and observations: Results from mesoscale to internal wave frequencies. *Journal of Geophysical Research: Oceans*, *125*(5), e2019JC015306. https://doi.org/10.1029/2019JC015306

McComas, C. H., & Bretherton, F. P. (1977). Resonant interaction of oceanic internal waves. *Journal of Geophysical Research*, *82*(9), 1397–1412. https://doi.org/10.1029/jc082i009p01397

Morozov, E. (2006). Internal tides. Global field of internal tides and mixing caused by internal tides. In J. Grue & K. Trulsen (Eds.), *Waves in geophysical fluids* (Vol. 489, pp. 271–332). CISM International Centre for Mechanical Sciences. https://doi.org/10.1007/978-3-211-69356-8_6

Morrow, R., Fu, L.-L., Ardhuin, F., Benkiran, M., Chapron, B., Cosme, E., et al. (2019). Global observations of fine-scale ocean surface topography with the surface water and ocean topography (SWOT) mission. *Frontiers in Marine Science*, *6*, 232. https://doi.org/10.3389/fmars.2019.00232

Müller, P., Holloway, G., Henyey, F. S., & Pomphrey, N. (1986). Nonlinear interactions among internal gravity waves. *Reviews of Geophysics*, *24*(3), 493–536. https://doi.org/10.1029/rg024i003p00493

Munk, W., & Wunsch, C. (1998). Abyssal recipes II: Energetics of tidal and wind mixing. *Deep Sea Research Part I: Oceanographic Research Papers*, *45*(12), 1977–2010. https://doi.org/10.1016/S0967-0637(98)00070-3

Nelson, A. D., Arbic, B. K., Zaron, E. D., Savage, A. C., Richman, J. G., Buijsman, M. C., & Shriver, J. F. (2019). Toward realistic nonstationarity of semidiurnal baroclinic tides in a hydrodynamic model. *Journal of Geophysical Research: Oceans*, *124*(9), 6632–6642. https://doi.org/10.1029/2018JC014737

Ngodock, H. E., Souopgui, I., Wallcraft, A. J., Richman, J. G., Shriver, J. F., & Arbic, B. K. (2016). On improving the accuracy of the M2 barotropic tides embedded in a high-resolution global ocean circulation model. *Ocean Modelling*, *97*, 16–26. https://doi.org/10.1016/j.ocemod.2015.10.011

Niwa, Y., & Hibiya, T. (2001). Numerical study of the spatial distribution of the M_2 internal tide in the Pacific Ocean. *Journal of Geophysical Research*, *106*(C10), 22441–22449. https://doi.org/10.1029/2000JC000770

Niwa, Y., & Hibiya, T. (2004). Three-dimensional numerical simulation of M2 internal tides in the East China Sea. *Journal of Geophysical Research*, *109*(C4), C04027. https://doi.org/10.1029/2003JC001923

Niwa, Y., & Hibiya, T. (2011). Estimation of baroclinic tide energy available for Deep Ocean mixing based on three-dimensional global numerical simulations. *Journal of Oceanography*, *67*(4), 493–502. https://doi.org/10.1007/s10872-011-0052-1

Olbers, D. J. (1976). Nonlinear energy transfer and the energy balance of the internal wave field in the Deep Ocean. *Journal of Fluid Mechanics*, *74*(02), 375–399. https://doi.org/10.1017/s0022112076001857

OSiRIS. (2024). HYCOM sea surface height data from 2017 to 2019 (EXPT 21.6) [Dataset]. *OSiRIS*. Retrieved from https://app.globus.org/file-manager

Pan, Y., Arbic, B. K., Nelson, A. D., Menemenlis, D., Peltier, W. R., Xu, W., & Li, Y. (2020). Numerical investigation of mechanisms underlying oceanic internal gravity wave power-law spectra. *Journal of Physical Oceanography*, *50*(9), 2713–2733. https://doi.org/10.1175/JPO-D-20-0039.1

Polzin, K. L., Toole, J. M., & Schmitt, R. W. (1995). Finescale parameterizations of turbulent dissipation. *Journal of Physical Oceanography*, *25*(3), 306–328. https://doi.org/10.1175/1520-0485(1995)025⟨0306:fpotd⟩2.0.co;2

Qiu, B., Chen, S., Klein, P., Wang, J., Torres, H., Fu, L.-L., & Menemenlis, D. (2018). Seasonality in transition scale from balanced to unbalanced motions in the world ocean. *Journal of Physical Oceanography*, *48*(3), 591–605. https://doi.org/10.1175/JPO-D-17-0169.1

Ray, R. D., Egbert, G., & Erofeeva, S. (2005). A brief overview of tides in the Indonesian seas. *Oceanography*, *18*(4), 74–79. https://doi.org/10.5670/oceanog.2005.07

Ray, R. D. (1999). *A global ocean tide model from TOPEX/POSEIDON altimetry: GOT99.2*. National Aeronautics and Space Administration, Goddard Space Flight Center. Google-Books-ID: iEQ7AQAAMAAJ.

Ray, R. D., & Mitchum, G. T. (1996). Surface manifestation of internal tides generated near Hawaii. *Geophysical Research Letters*, *23*(16), 2101–2104. https://doi.org/10.1029/96gl02050

Ray, R. D., & Mitchum, G. T. (1997). Surface manifestation of internal tides in the deep ocean: Observations from altimetry and island gauges. *Progress in Oceanography*, *40*(1–4), 135–162. https://doi.org/10.1016/s0079-6611(97)00025-6

Richman, J. G., Arbic, B. K., Shriver, J. F., Metzger, E. J., & Wallcraft, A. J. (2012). Inferring dynamics from the wavenumber spectra of an eddying global ocean model with embedded tides. *Journal of Geophysical Research*, *117*(C12), C12012. https://doi.org/10.1029/2012JC008364

Robertson, R., & Ffield, A. (2008). Baroclinic tides in the Indonesian seas: Tidal fields and comparisons to observations. *Journal of Geophysical Research*, *113*(C7), C07031. https://doi.org/10.1029/2007JC004677

Rocha, C. B., Chereskin, T. K., Gille, S. T., & Menemenlis, D. (2016). Mesoscale to submesoscale wavenumber spectra in Drake Passage. *Journal of Physical Oceanography*, *46*(2), 601–620. https://doi.org/10.1175/JPO-D-15-0087.1

Savage, A. C., Arbic, B. K., Alford, M. H., Ansong, J. K., Farrar, J. T., Menemenlis, D., et al. (2017). Spectral decomposition of internal gravity wave sea surface height in global models. *Journal of Geophysical Research: Oceans*, *122*(10), 7803–7821. https://doi.org/10.1002/2017JC013009

Shriver, J. F., Arbic, B. K., Richman, J. G., Ray, R. D., Metzger, E. J., Wallcraft, A. J., & Timko, P. G. (2012). An evaluation of the barotropic and internal tides in a high-resolution global ocean circulation model. *Journal of Geophysical Research*, *117*(C10), C10024. https://doi.org/10.1029/2012JC008170

Skitka, J., Arbic, B. K., Thakur, R., Menemenlis, D., Peltier, W. R., Pan, Y., et al. (2023). Probing the nonlinear interactions of supertidal internal waves using a high-resolution regional ocean model. *Journal of Physical Oceanography*, *54*(2), 399–425. https://doi.org/10.1175/JPO-D-22-0236.1

Solano, M., Buijsman, M., Shriver, J., Magalhaes, J., da Silva, J., Jackson, C., et al. (2023). Nonlinear internal tides in a realistically forced global ocean simulation (preprint). *Physical Sciences*. https://doi.org/10.20944/preprints202308.0856.v1

Stammer, D. (1997). Global characteristics of ocean variability estimated from regional TOPEX/POSEIDON altimeter measurements. *Journal of Physical Oceanography*, *27*(8), 1743–1769. https://doi.org/10.1175/1520-0485(1997)027⟨1743:gcoove⟩2.0.co;2

Stammer, D. & Cazenave, A. (Eds.) (2017). *Satellite altimetry over oceans and land surfaces*. CRC Press. https://doi.org/10.1201/9781315151779

Tchilibou, M., Gourdeau, L., Lyard, F., Morrow, R., Koch Larrouy, A., Allain, D., & Djath, B. (2020). Internal tides in the Solomon Sea in contrasted ENSO conditions. *Ocean Science*, *16*(3), 615–635. https://doi.org/10.5194/os-16-615-2020

Torres, H. S., Klein, P., Menemenlis, D., Qiu, B., Su, Z., Wang, J., et al. (2018). Partitioning ocean motions into balanced motions and internal gravity waves: A modeling study in anticipation of future space missions. *Journal of Geophysical Research: Oceans*, *123*(11), 8084–8105. https://doi.org/10.1029/2018JC014438

Whalen, C. B., MacKinnon, J. A., Talley, L. D., & Waterhouse, A. F. (2015). Estimating the mean diapycnal mixing using a finescale strain parameterization. *Journal of Physical Oceanography*, *45*(4), 1174–1188. https://doi.org/10.1175/jpo-d-14-0167.1

Wunsch, C. (1975). Internal tides in the ocean. *Reviews of Geophysics*, *13*(1), 167–182. https://doi.org/10.1029/rg013i001p00167

Yadidya, B. (2023). Replication data for: "Phase-accurate internal tides in a global ocean forecast model: Potential applications for nadir and wide-swath altimetry" [Dataset & Software]. Harvard Dataverse. https://doi.org/10.7910/DVN/HMDTRZ

Yadidya, B., & Rao, A. D. (2022a). Interannual variability of internal tides in the Andaman sea: An effect of Indian ocean dipole. *Scientific Reports*, *12*(1), 11104. https://doi.org/10.1038/s41598-022-15301-8

Yadidya, B., & Rao, A. D. (2022b). Projected climate variability of internal waves in the Andaman Sea. *Communications Earth & Environment*, *3*(1), 252. https://doi.org/10.1038/s43247-022-00574-8

Yadidya, B., Rao, A. D., & Latha, G. (2022). Investigation of internal tides variability in the Andaman sea: Observations and simulations. *Journal of Geophysical Research: Oceans*, *127*(4), e2021JC018321. https://doi.org/10.1029/2021JC018321

Yu, X., Ponte, A., Elipot, S., Menemenlis, D., Zaron, E. D., & Abernathey, R. P. (2019). Surface kinetic energy distributions in the global oceans from a high-resolution numerical model and surface drifter observations. *Geophysical Research Letters*, *46*(16), 9757–9766. https://doi.org/10.1029/2019gl083074

Zaron, E. D. (2017). Mapping the nonstationary internal tide with satellite altimetry. *Journal of Geophysical Research: Oceans*, *122*(1), 539–554. https://doi.org/10.1002/2016JC012487

Zaron, E. D. (2019). Baroclinic tidal sea level from exact-repeat mission altimetry. *Journal of Physical Oceanography*, *49*(1), 193–210. https://doi.org/10.1175/JPO-D-18-0127.1

Zaron, E. D. (2022). Baroclinic tidal cusps from satellite altimetry. *Journal of Physical Oceanography*, *52*(12), 3123–3137. https://doi.org/10.1175/JPO-D-21-0155.1

Zaron, E. D., & Ray, R. D. (2023). Clarifying the distinction between steric and baroclinic sea surface height. *Journal of Physical Oceanography*, *53*(11), 2591–2596. https://doi.org/10.1175/JPO-D-23-0073.1

Zhao, Z. (2023). Mode-1 N_2 internal tides observed by satellite altimetry. *Ocean Science*, *19*(4), 1067–1082. https://doi.org/10.5194/os-19-1067-2023

Zhao, Z., Alford, M. H., MacKinnon, J. A., & Pinkel, R. (2010). Long-range propagation of the semidiurnal internal tide from the Hawaiian Ridge. *Journal of Physical Oceanography*, *40*(4), 713–736. https://doi.org/10.1175/2009JPO4207.1

Zhao, Z., & Qiu, B. (2023). Seasonal West-east seesaw of M_2 internal tides from the Luzon Strait. *Journal of Geophysical Research: Oceans*, *128*(3), e2022JC019281. https://doi.org/10.1029/2022JC019281